

A photometric study of faint galaxies in the field of GRB 000926

© 2004 T.A.Fatkhullin¹, A.A.Vasil'ev², V.P.Reshetnikov²

¹ Special Astrophysical Observatory, Russian Academy of Sciences, Nizhnii Arkhyz, 357147 Karachai-Cherkessian Republic, Russia

² Astronomical Institute of St.Petersburg State University, Universitetskii pr. 28, Petrodvoretz, 198504 Russia

We present our B , V , R_c , and I_c observations of a $3.6' \times 3'$ field centered on the host galaxy of GRB 000926 ($\alpha_{2000.0}=17^h04^m11^s$, $\delta_{2000.0}=+51^\circ47'9.8''$). The observations were carried out on the 6-m Special Astrophysical Observatory telescope using the SCORPIO instrument. The catalog of galaxies detected in this field includes 264 objects for which the signal-to-noise ratio is larger than 5 in each photometric band. The following limiting magnitudes in the catalog correspond to this limitation: 26.6(B), 25.7(V), 25.8(R_c), and 24.5(I_c). The differential galaxy counts are in good agreement with previously published CCD observations of deep fields. We estimated the photometric redshifts for all of the cataloged objects and studied the color variations of the galaxies with z . For luminous spiral galaxies with $M(B) < -18$, we found no evidence for any noticeable evolution of their linear sizes to $z \sim 1$.

Keywords: distant galaxies, photometric observations

1. Introduction

In recent years, significant progress has been made in studying the properties and evolution of distant galaxies. An important role in this progress has been played by detailed studies of several so-called deep fields – relatively small areas imaged (generally in several color bands) with long exposure times. The best-known deep fields include the northern and southern fields of the Hubble Space Telescope (Ferguson et al. 2000), Subaru (Maihara et al. 2001), VLT FORS (Heidt et al. 2003), and the most recent and deepest (in the history of optical astronomy) survey conducted as part of the GOODS (Great Observatories Origins Deep Survey) project with the Hubble Space Telescope (Giavalisco et al. 2003). In addition to surveys covering an appreciable part of the sky (2MASS, 2dF, SDSS, and others), but limited to relatively low redshifts ($z \leq 0.3$), deep fields allow the properties of high z galaxies to be studied and provide information about the evolution of the integrated parameters of galaxies.

Our primary objective was to study in detail the faint galaxies distinguished in the deep field obtained with the 6-m Special Astrophysical Observatory (SAO) telescope as part of our program of optical identification of gamma-ray bursts (GRBs). In recent years, investigators have increasingly pointed out that, with the accumulation of observational data, GRBs with their afterglows and host galaxies are becoming a useful tool in observational cosmology (see, e.g., Djorgovski et al. 2003; Ramirez-Ruiz et al. 2001; Trentham et al. 2002; and references therein). Thus, a comparative analysis of the properties of GRB host galaxies with the properties of galaxies at the same redshifts is now of relevant interest. One of the methods for solving this problem is to study the population of faint galaxies in the deep fields of GRB host galaxies.

2. Observations and data reduction

We carried out our photometric observations of the field of the host galaxy of GRB 000926 on July 24 and 25, 2001, using the 6-m SAO telescope. The ob-

serving conditions were photometric with 1.3-arcsec seeing, measured as the full width at half maximum (FWHM) of the images of starlike objects in the field. The field was centered on the coordinates of the host galaxy $\alpha_{2000.0}=17^h04^m11^s$, $\delta_{2000.0}=+51^\circ47'9.8''$, which correspond to the Galactic latitude and longitude $b = 37^\circ21'$ and $l = 77^\circ45'$, respectively. According to the infrared maps taken from the paper by Schlegel et al. (1998), the Galactic reddening toward the field being studied is $E(B - V)=0.023$.

In our observations, we used the SCORPIO (Spectral Camera with Optical Reducer for Photometrical and Interferometrical Observations; for a description, see <http://www.sao.ru/moisav/scorpio/scorpio.html>) instrument mounted at the prime focus of the 6-m SAO telescope. The detector was a TK1024 1024×1024 CCD array. The pixel size was 24 μm , which corresponded to an angular scale of 0.289'' per pixel. The CCD response curve and the SCORPIO broad-band filters reproduced a photometric system close to the standard Johnson–Cousins BVR_cI_c system (Bessel 1990). We took five frames in each of the B and V bands with total exposure times of 2500^s and 1500^s, respectively; ten frames in R_c (1800^s); and fifteen frames in I_c (1800^s). The absolute photometric calibration of the data was performed using the observations of standard stars from the lists by Landolt (1992) and Stetson (accessible at <http://cadwww.dao.nrc.ca/cadcbn/wdb/astro-cat/stetson/query>) on the same nights.

The primary data reduction was performed using the ESO-MIDAS¹ software package. It included de-biasing, flat fielding, defringing in R_c and I_c , and cosmic-ray hit removal (for a detailed description, see the dissertation by Fatkhullin 2003). All of the frames taken in one color band were coadded. The coadded frames were reduced to the same orientation and to a single coordinate system. The sizes of the region where the coadded images overlapped in all bands were $3.6' \times 3'$. This region was used for the subsequent analysis (Fig. 1).

3. Large-scale photometry of objects in the field

3.1. Extracting objects

We used the SExtractor (Source Extractor) (Bertin and Arnouts 1996) package to extract objects in the field and to perform their photometry. This package is unique in that it allows us to extract objects and construct their isophotes on one image and to calculate the fluxes within these isophotes on another image. Thus, we can determine the fluxes in all bands for a given object within the same region of the image. On the other hand, this technique makes it possible to find all of the objects in the field from its common image for all bands, which allows problems with the identification of the same object in different bands to be avoided.

There are several methods for constructing a common image (i.e., the detection field). For example, the field obtained by coadding the frames in different color bands is often used to extract objects. We used a relatively new method, that of constructing a χ^2 -field. The χ^2 -field is a common image for all bands, and it is used to extract objects and to construct a common catalog of objects for all bands. The idea of the method is that probabilistic methods are used to analyze the distribution of image pixel values and to determine the optimum detection limit for objects above the background level (Szalay et al. 1999).

Schematically, the process of constructing the χ^2 -field can be described as follows. The mean and rms deviation (σ_b) of the sky background (the distribution of sky background values is assumed to be Gaussian) are determined from the images in each color band. Subsequently, the corresponding background value is subtracted from each image, and the resulting frame is divided by σ_b . As a result, we obtain a transformed image for each band in which the sky background is specified by a Gaussian with a zero mean and a unit variance. If we consider the combined transformed images, each pixel of the common field may be represented as a vector with the number of elements equal to the number of bands. The resulting χ^2 -field is an image, each pixel of which is equal to the square of the length of the corresponding vector of the common field.

If the observed region contained no objects and displayed only the sky background, then the probability distribution function for χ^2 -field values would correspond to χ^2 with the number of degrees of freedom equal to the number of bands. However, an ac-

¹ This package is supported and distributed by the European Southern Observatory.

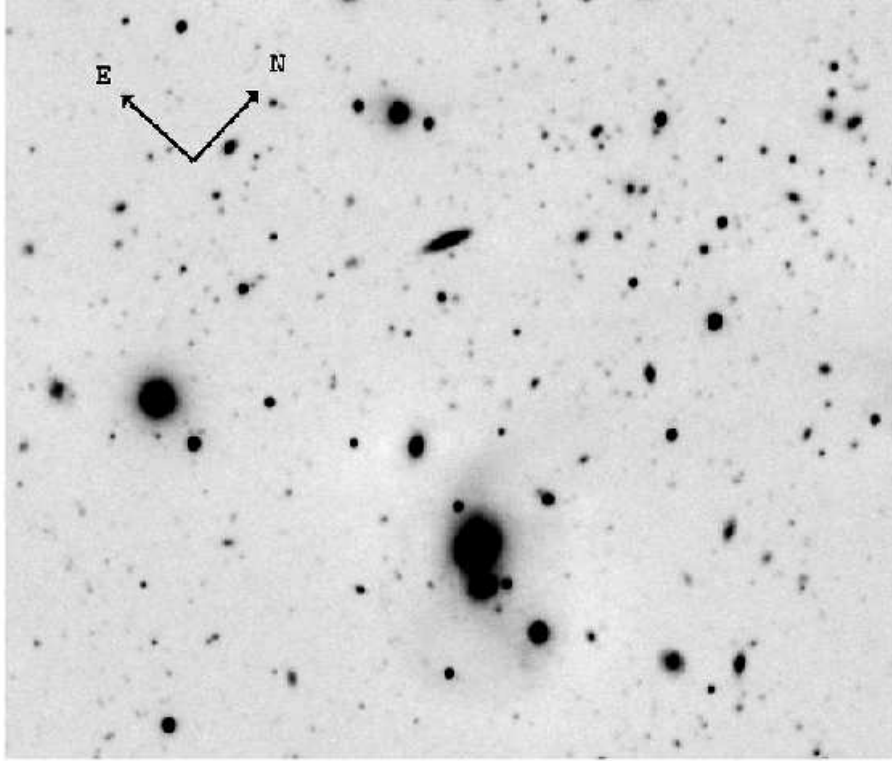


Fig. 1. Reproduction of the field of GRB 000926. The field sizes are $3.6' \times 3'$.

tual field contains objects, and, therefore, the distribution of χ^2 -field values is distorted. By analyzing the χ^2 -fields for the observed region and for the sky background, we can determine the optimum detection limit for objects in the actual field; this limit turns out to be lower than that in the method of coadding the frames in different color bands.

The detection conditions were specified in such a way that objects that occupied an area of no less than five pixels were extracted at fluxes in these pixels exceeding 3σ above the background level. For detection, we also used filtering based on a wavelet analysis using a mexhat-type filter with a FWHM that corresponded to the quality of our images, i.e., $1.3''$. This filtering allowed us to effectively extract objects in frames with a large image density and around bright extended galaxies as well as to separate the components of multiple objects.

3.2. Object extraction results and photometry

More than 550 objects satisfied the detection criteria. However, to eliminate problems related to inaccurate photometry due to the defects of the objects themselves, we excluded those which turned out to be near the image boundaries and in two regions around very

bright objects (an overexposed star and a large interacting system of galaxies). Thus, slightly more than 400 objects remained.

To increase the reliability of the subsequent analysis, we included in the final catalog only those objects for which the signal-to-noise ratio was larger than 5 in each band. There were 285 such objects. The following limiting magnitudes in the catalog corresponded to this limitation: 26.6 (B), 25.7 (V), 25.8 (R_c), and 24.5 (I_c).

For each object, we determined the total apparent magnitudes and the corresponding color indices using the so-called best magnitudes generated by the SExtractor package. These values are the best fits to the asymptotic magnitudes of extended objects (Bertin and Arnouts 1996).

The SExtractor package allows the objects to be separated into starlike and extended ones by assigning a corresponding “stellarity index” from 0 (extended) to 1 (star) to each of them. For the subsequent analysis, we selected only those objects for which the stellarity index was less than 0.7 in B (in this band, the stellar disks and spiral arms of galaxies are separated relatively better). There were 264 such objects. We attributed the objects with an index larger than 0.7 (their number was 21) to stars.

4. Estimating the redshifts

Determining the spectroscopic redshifts for several hundred faint objects extracted in deep fields is a complicated and time-consuming observational problem. Fortunately, for many problems (e.g., for estimating the evolution of the galaxy luminosity function), the so-called photometric redshifts estimated from multicolor photometry turn out to be quite acceptable. The accuracy of these z estimates is about 10%, which is high enough for statistical studies of the properties of distant objects. The main idea of the photometric redshift estimation is very simple: an object's multicolor photometry may be considered as a low-resolution spectrum that is used to estimate z (Baum 1963).

In practice, we estimated the photometric redshifts for the extended objects of our sample using the Hyperz software package (Bolzonella et al. 2000). The input data for Hyperz were: the apparent magnitudes of the objects in four bands, the internal extinction law (we used the law by Calzetti et al. (2000) for starburst galaxies, which is most commonly used for studies similar to our own), the redshift range in which the solution is sought (we considered z from 0 to 1.3), and the cosmological model (we used a flat model with $\Omega_m=0.3$, $\Omega_\Lambda=0.7$, and $H_0=70$ km/s/Mpc). The observed spectra of the galaxies were compared with the synthetic spectra for E, Sa, Sc, Im, and starburst galaxies taken from the GISSEL98 library.

Apart from the redshift estimate, the Hyperz package yielded the following basic parameters for each object: the spectral type of the galaxy (based on the similarity between the spectral energy distribution of the object and one of the synthetic spectra), the age, the absolute B magnitude, and a number of others.

5. Results and discussion

Our catalog of extended objects ($N=264$) has the following integrated parameters:

(1) the mean absolute magnitude of the galaxies is $M_B = -17.4 \pm 2.7$ (σ);

(2) the mean photometric redshift is $\langle z \rangle = 0.53 \pm 0.39$;

(3) the stellarity index in the B band is 0.08 ± 0.12 , i.e., extended objects dominate in the catalog;

(4) the apparent flattening of the galaxies varies between 0.22 and 1.00 with a mean value of $\langle b/a \rangle = 0.80 \pm 0.20$.

Irregular and starburst galaxies (126 of the 264 objects or 48%) constitute about one half of the catalog. Sa–Sc spiral galaxies are encountered in almost a third of the cases (79 objects or 30%). The contribution of elliptical galaxies is 22% (59 objects).

The mean angular size of the objects (FWHM) corrected for the FWHM of the stars varies between $1.0''$ in R_c to $1.2''$ in I_c (the errors of the means are $\pm 0.5''$). At the mean redshift, a linear size of ≈ 7 kpc corresponds to this angular size. If we restrict our analysis to relatively near galaxies at $z \leq 0.5$ (in this case, the mean redshifts of the galaxies of various spectral types are close), the expected dependence of the linear sizes on the galaxy type shows up. Thus, the mean FWHM for elliptical galaxies corresponds to a linear size of 3.4 kpc, while starburst galaxies exhibit more extended brightness distribution with FWHM ≈ 4.7 kpc.

5.1. Starlike objects

We used a fairly stringent criterion to separate galaxies and stars: we attributed objects with a stellarity index in B of less than 0.7 to galaxies (a less stringent limitation, e.g., 0.9–0.95 (Arnouts et al. 2001), is commonly used).

The number of stars found in the field (21 stars with apparent magnitudes $B \leq 24.5$) is in good agreement with the prediction of Bezanon's Milky Way model (for a description of this model, see, e.g., Robin et al. 2000). In a field with an area of 0.003 square degrees located at the Galactic coordinates that correspond to our region, this model predicts 24 stars with $B \leq 24.5$. Given the small size of the field under study, such a close coincidence is, of course, partly accidental. However, it is indicative of the relatively small number of stars that could be erroneously attributed to galaxies.

Figure 2 shows the distribution of stars in the two-color diagram. The solid line in the figure represents the color sequence for main sequence stars (Sparke and Gallagher 2000). Most of the stars exhibit colors typical of main-sequence dwarfs.

5.2. Galaxy counts

The differential galaxy counts normalized to 1 sq. degree and found within $0^m.5$ bins are shown in Fig. 3 (circles). These counts were not corrected for observational selection and represent the actually observed numbers. The crosses in the figure indicate

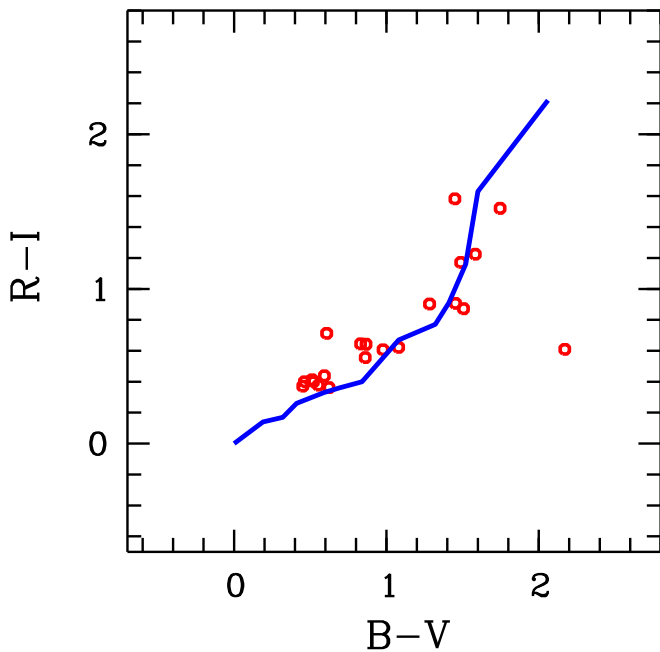


Fig. 2. Color distribution for starlike objects in the two-color diagram. The solid line represents the color sequence for main sequence stars.

similar counts for the VIRMOS survey (Le Fevre 2003; McCracken et al. 2003). Clearly, our counts are in excellent agreement with this survey. For apparent magnitudes $B < 25$, $V < 24.5$, $R_c < 24$, and $I_c < 24$, the difference in the numbers of galaxies observed in one magnitude bin, on average, does not exceed 20%. For fainter magnitudes, observational selection, which manifests itself in the form of bends in the curves of differential counts in Fig. 3, strongly affects our data.

The slopes of the curves shown in Fig. 3 are also in good agreement. According to our data, these slopes are

0.47 ± 0.09 ($B \leq 25$), 0.47 ± 0.04 ($V \leq 24$),
 0.38 ± 0.03 ($R_c \leq 24$) and 0.29 ± 0.04 ($I_c \leq 24$).
 A similar variation in the slopes of the curves of differential counts when passing from B to I_c was also pointed out by McCracken et al. (2003).

On the other hand, the VIRMOS data are in excellent agreement (to within 10%) with previous CCD galaxy counts (McCracken et al. 2003). As an example, Fig. 3 shows the counts for the northern and southern deep fields of the Hubble Space Telescope (Metcalf et al. 2001). Near $B \sim 25$, the ground-based and space counts join to form a single dependence that is currently traceable to $B \sim 29$. A detailed interpretation of this dependence (apart from

the fact that this is a classical cosmological test) can yield important information about the evolution of galaxy properties (Gardner 1998).

In Fig. 4, the observed colors of our field galaxies are plotted against their apparent magnitude. The figure clearly shows a trend well known from previous studies: fainter galaxies have, on average, bluer colors. The dashed lines in the figure indicate similar dependences for the VIRMOS galaxies (McCracken et al. 2003) that are in satisfactory agreement with our data.

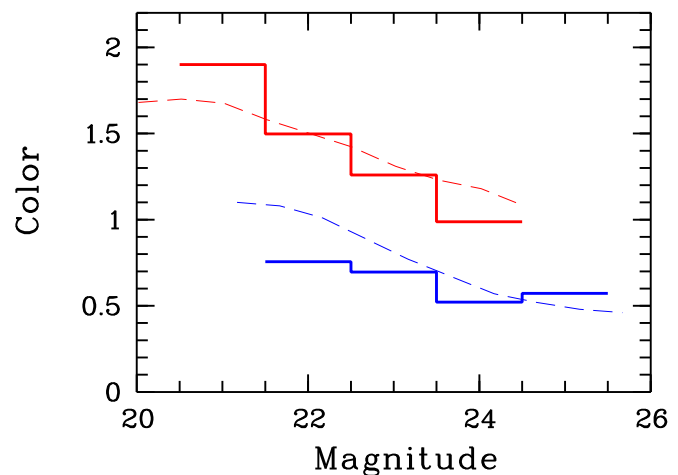


Fig. 4. Mean color index $V - I_c$ for the galaxies of our field versus apparent magnitude I_c (red), and color index $B - V$ versus B (blue). The dashed lines represent similar diagrams for the VIRMOS galaxies (McCracken et al. 2003).

The agreement between the counts in our field with the data for other deep fields is remarkable, because our field is very small and contains a relatively small number of galaxies. For example, the previously mentioned VIRMOS catalog contains $\approx 10^5$ galaxies; this number exceeds the size of our sample by several hundred. This agreement suggests that our field is representative and reflects well the average properties of the galactic population, at least up to $z \sim 1$.

5.3. The z distribution

Figure 5 (left) shows the redshift distribution of the catalogued galaxies. This distribution exhibits a peak at $z = 0.2 - 0.3$ and a long, gently sloping tail up to $z = 1.3$. The z distribution of the galaxies is distorted by selection effects. One of the strongest selection effects is our requirement that the signal-to-noise ratio for an object be larger than five in all

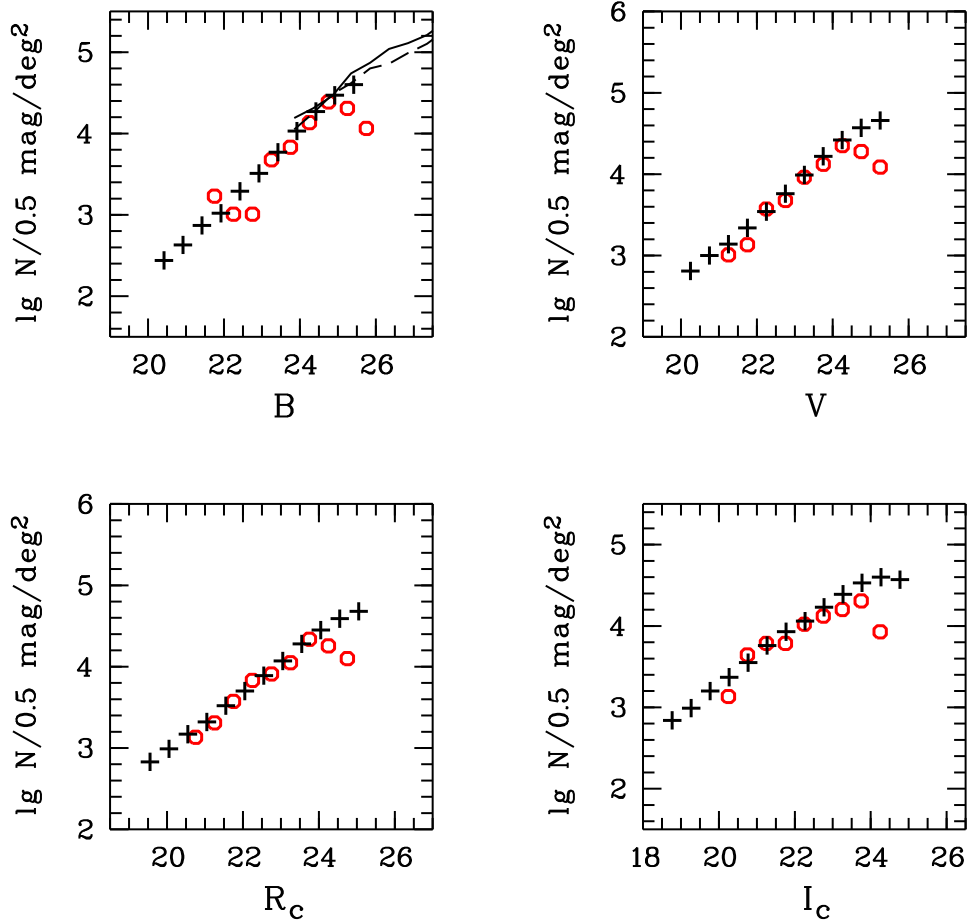


Fig. 3. Differential galaxy counts in the field of GRB 000926 (circles) in different bands. The crosses indicate similar counts for the VIRMOS survey (McCracken et al. 2003). The solid and dashed lines represent the B -band counts for the northern and southern deep fields of the Hubble Space Telescope, respectively (Metcalf et al. 2001).

four bands. As a result of this condition, early-type objects were mostly detected at a relatively low z because of the decline in the spectral energy distribution of early-type galaxies at short wavelengths. This effect is clearly seen from Fig. 5 (left), where the dashed and heavy solid lines indicate the distributions of E–Sa and Sc–Im galaxies, respectively.

Figure 5 (right) shows the distribution of the catalogued galaxies in the "absolute magnitude ($M(B)$) – redshift" plane. The galaxy distribution in this plane is also determined by selection effects; we extract mostly luminous objects among the more distant objects. As an example, the dashed line in the figure indicates the selection curve for an Sc spiral galaxy with the apparent magnitude $B = 26$ (the observed magnitude distorted by the k -correction). If all of the galaxies of this type brighter than 26^m were included in our sample of objects, they would lie below the dashed line in the figure. The fainter galaxies with

$B > 26$ would lie above this line. Clearly, the magnitude limitation explains well the galaxy distribution in the $M(B) - z$ plane.

The strong selection in absolute magnitude in our sample makes it difficult to directly compare the parameters of nearby and distant galaxies. However, if we restrict our analysis only to luminous objects (say, with $M(B) < -18$), then the selection effect is weaker for them, and such galaxies are confidently extracted up to the limiting z of our sample (Fig. 5). Spiral and starburst galaxies dominate (90%) in this sample.

Figure 6 shows variations in the angular sizes (the FWHM corrected for the FWHM of the stars) of luminous ($M(B) < -18$) galaxies in the R_c band (the seeing was best during observations in this band). Note that the FWHM values depend on the cosmological dimming in brightness much less strongly than do the isophotal diameters. Therefore, they may

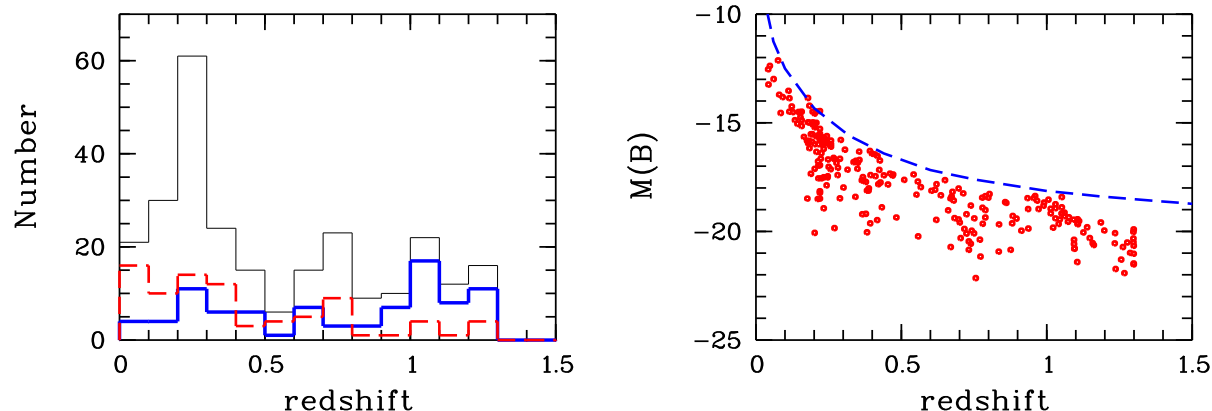


Fig. 5. The z distribution of sample galaxies (thin solid line); the heavy solid (blue) and dashed (red) lines indicate the distributions for Sc-Im and E-Sa galaxies, respectively (left). The absolute magnitude – redshift diagram (right).

be used as rough estimates of the galaxy sizes. The barred circles in Fig. 6 represent the mean values and the corresponding dispersions for the redshift ranges 0–0.5, 0.5–1.0, and 1.0–1.3, while the dashed lines indicate the lines of constant linear sizes (the lower and upper curves correspond to linear sizes of 3 and 15 kpc, respectively). The angular sizes of the extended objects from our sample are located, on average, between the two curves of constant linear sizes. For the luminous galaxies under consideration, the mean FWHM in linear measure changes only slightly with increasing z , and is 8 kpc (the solid curve in Fig. 6). The dotted curve in Fig. 6 indicates the expected variation in the observed angular size of an object 8 kpc in diameter, as predicted by the model by Mao et al. (1998) (in this model, the galaxy size varies as $\propto (1+z)^{-1}$). Clearly, our data for the galaxies with $M(B) < -18$ are inconsistent with such a strong evolution of their sizes. This conclusion agrees with the conclusion by Lilly et al. (1998) that the linear sizes of large and luminous spiral galaxies change little to $z \sim 1$. A similar conclusion was reached by Simard et al. (1999) and Takamiya (1999).

In the redshift range 0.3 to 0.5, where faint and luminous objects are represented almost equally, we compared the linear sizes for the galaxies with $M(B) > -18$ and $M(B) < -18$. The luminous ($M(B) \approx -19$) spiral and elliptical galaxies turned out to be a factor of about 1.5 to 2 larger than the fainter ($M(B) \approx -17$) galaxies. The expected change in size for a galaxy with an exponential brightness distribution and a constant central surface brightness is $\Delta \log D \propto 0.2 \Delta M$. Therefore, when the absolute magnitude of a spiral galaxy changes by 2^m , its size

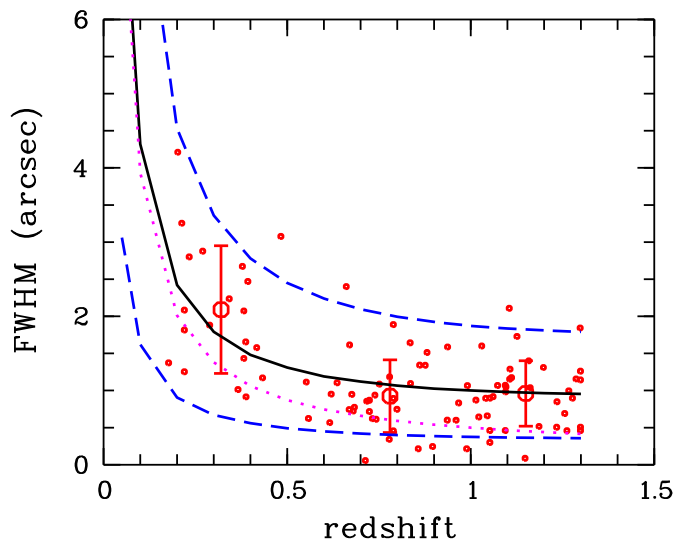


Fig. 6. Galaxy angular size in R_c versus redshift (see the text).

will change by a factor of ≈ 2.5 . The observed change in galaxy size is smaller than this estimate, probably because the disks of many distant galaxies are poorly described by an exponential law (Reshetnikov et al. 2003).

The variation in the observed colors of extended objects with z roughly corresponds to the expected variation for local galaxies at the corresponding z . As an example, Fig. 7a,b shows the galaxy positions in the two-color diagrams for two redshift ranges. The solid line in each of the panels represents the color sequence for normal galaxies at $z = 0.2$ (a) and $z = 0.8$ (b), as constructed by Fukugita et al. (1995). The colors of galaxies at $z = 0.7 - 0.9$ are in satisfac-

tory agreement with the expected distribution in the two-color diagram (all of the objects in this z range brighter than $M(B) = -18$); the agreement is poorer for $z \approx 0.2$. However, the agreement becomes much better if we consider only the luminous galaxies with $M(B) < -18$ at $z \approx 0.2$ (the crosses in Fig. 7a).

The color variations of Sa–Im spiral galaxies with z are shown in a more detailed form in Figs. 7c and 7d. The solid lines in these figures represent the expected dependences for the accretion model of spiral galaxy formation (Westera et al. 2002; Samland and Gerhard 2003). According to Westera et al. (2002), the galactic disk is formed inside a dark halo through ongoing external gas accretion. In this model, the star formation rate is a nonmonotonic function of time: it reaches its maximum at $z \approx 1$ and remains significant down to $z = 0$. The dashed lines indicate the dependences for the model of a single collapse. In this scenario, the disk has been formed through the contraction of a protogalactic cloud at $z > 1$. We see from Figs. 7c and 7d that, in general, the accretion model satisfactorily describes the general pattern of variation in the observed colors of galaxies with z . The collapse model is in much poorer agreement with our data, predicting much redder colors at each z .

5.4. The host galaxy of GRB 000926

What is the host galaxy of the GRB whose region is studied here?² The apparent magnitudes of the galaxy corrected for extinction in the Milky Way are $B = 26.01 \pm 0.17$, $V = 25.76 \pm 0.22$, $R_c = 25.88 \pm 0.28$, and $I_c = 24.65 \pm 0.40$ (Fatkhullin 2002); its redshift is $z = 2.0379$ (Castro et al. 2003). Given the k -correction for an Sc spiral galaxy (Poggianti 1997), the absolute magnitude of the host galaxy is $M(B) = -19.1$. Consequently, it is a relatively faint, but not dwarf object. The galaxy mass was roughly estimated by Castro et al. (2003) to be $\approx 10^{10} M_\odot$. This value yields an estimate of the mass-to-light ratio $M/L(B) \approx 1.5$ (in solar units), which is typical of objects of late morphological types with enhanced star formation.

The observed colors of the host galaxy were compared with the colors of faint ($B > 25$) galaxies in this field by Fatkhullin (2002). The galaxy was found to be, on average, bluer than other faint extended objects. This conclusion is also confirmed by a direct

comparison of the observed colors for the host galaxy of GRB 000926 with the colors of objects at $z \approx 2$ in our field. Note, however, that, because of observational selection (see Fig. 5), the galaxies that we extracted at $z \approx 2$ are, on average, much more luminous than the host galaxy being discussed. A proper comparison of the colors requires studying the parameters of galaxies at $z \approx 2$ with a luminosity comparable to that of the GRB 000926 host galaxy. Since such objects are located near the magnitude limit of our field, this is very difficult to do using our data. However, certain conclusions can still be reached. That the colors of the host galaxy are bluer than the colors of galaxies at lower z can be explained by the fact that the specific star formation rate in the Universe increases with redshift (see, e.g., Madau et al. 1998); hence, bluer colors are expected, on average, for the galaxies (see, e.g., Fig. 3 from the paper by Rudnik et al. 2003). Therefore, the host galaxy may well be a typical spiral galaxy for an epoch of $z \approx 2$. This explanation is consistent with the conclusion previously reached by several authors that the host galaxies of GRBs are normal blue galaxies similar in properties to galaxies at the same redshifts (Sokolov et al. 2001; Le Floc’h et al. 2003; Djorgovski et al. 2003).

6. Conclusions

We have presented the results of our detailed photometric study of a small ($3.6' \times 3'$) region in the field of GRB 000926 (Fig. 1). The observations were carried out on good photometric nights, which allowed us to reach a limiting magnitude of 26.6 in the B band under fairly stringent conditions.

In the field under study, we extracted 264 extended objects and 21 starlike objects. The number of presumed stars agrees with the expected number in Bezanson’s Milky Way model. The stellar colors are typical of main sequence dwarfs (Fig. 2).

The differential galaxy counts in the field to $B \approx 25$ are in good (to within 20%) agreement with previous CCD surveys of several deep fields (Fig. 3). We have confirmed the existence of a general tendency in the observed colors of the field galaxies with their apparent magnitude (Fig. 4).

An analysis of the images of luminous ($M(B) < -18$) galaxies has led us to conclude that there is no strong evolution of their linear sizes at $z \leq 1$ (Fig. 6).

In general, the color variations of spiral galaxies with z agree with the predictions of the accretion

² An image of this galaxy and more information can be found at SAO RAS <http://www.sao.ru/hq/grb/host-obs.html>.

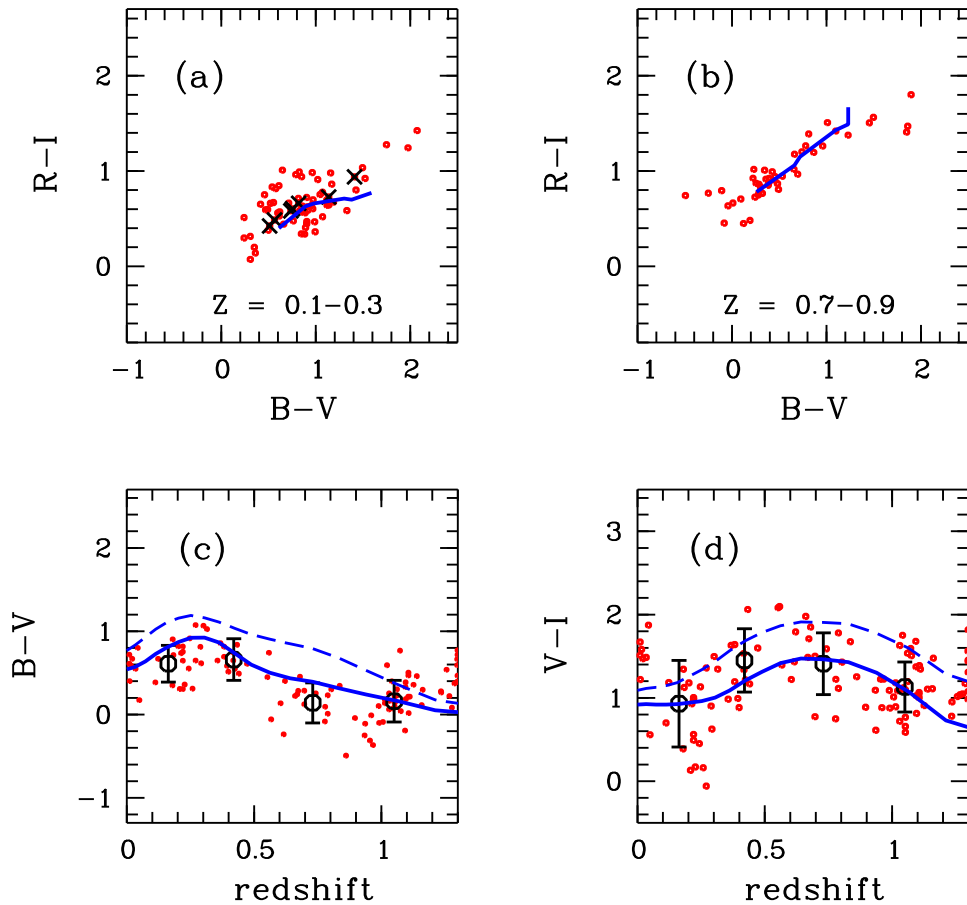


Fig. 7. (a and b) Positions of the sample galaxies in the two-color diagrams for two redshift ranges. The solid lines indicate the corresponding color sequences for normal galaxies (Fukugita et al. 1995); the crosses in Fig. 7a mark luminous galaxies with $M(B) < -18$. (c and d) The evolution of the observed colors of spiral galaxies. The barred circles represent the mean color indices in the redshift ranges 0–0.3, 0.3–0.6, 0.6–0.9, and 0.9–1.2. The heavy solid and dashed lines indicate the model dependences for the accretion model of disk galaxy formation and for the model of a single collapse (Westera et al. 2002), respectively.

model, in which galactic disks are formed within dark halos through long-term external gas accretion (Fig. 7).

One of the important results of our study is that in the cases where we can compare our data with previously published data for other (often deeper and larger) fields, they are in good agreement. This implies that investigating relatively small deep fields is a quite efficacious method of studying the evolution of galaxies.

Acknowledgments

This study was supported by the Federal Program “Astronomy” (project no. 40.022.1.1.1101) and the Russian Foundation for Basic Research (project nos. 03-02-17152 and 01-02-17106.

REFERENCES

- S. Arnouts, B. Vandame, C. Benoist, et al., *Astron. Astrophys.* 379, 740 (2001).
- W. Baum, *IAU Symp. 15: Problems of Extragalactic Research* (Macmillan, New York, 1963), p. 390.
- E. Bertin and S. Arnouts, *Astron. Astrophys.* 117, 393 (1996).
- M. Bessel, *Publ. Astron. Soc. Pac.* 102, 1181 (1990).
- M. Bolzonella, J.-M. Miralles, and R. Pello, *Astron. Astrophys.* 363, 476(2000).
- D. Calzetti, L. Armus, R. C. Bohlin, et al., *Astrophys. J.* 533, 682 (2000).
- S. Castro, T. Galama, F. Harrison, et al., *Astrophys. J.* 586, 128 (2003).

- S. G. Djorgovski, S. R. Kulkarni, D. A. Frail, et al., *Proc. SPIE* 4834, 238 (2003).
- T. Fatkhullin, *Bull. Spec. Astrophys. Obs.* 53, 5 (2002).
- T. A. Fatkhullin, Candidate's Dissertation (SAO RAS, Nizhnii Arkhyz, 2003); <http://www.sao.ru/hq/grb/team/timur/timur.html>.
- H. C. Ferguson, M. Dickinson, and R. Williams, *Ann. Rev. Astron. Astrophys.* 38, 667 (2000).
- M. Fukugita, K. Shimasaku, and T. Ichikawa, *Publ. Astron. Soc. Pac.* 107, 945 (1995).
- J. P. Gardner, *Publ. Astron. Soc. Pac.* 110, 291 (1998).
- M. Giavalisco et al. (the GOODS team), *astro-ph/0309105* (2003).
- J. Heidt, I. Appenzeller, A. Gabasch, et al., *Astron. Astrophys.* 398, 49 (2003).
- A. U. Landolt, *Astron. J.* 104, 340 (1992).
- O. Le Fevre, Y. Mellier, H. J. McCracken, et al., *astro-ph/0306252* (2003).
- E. Le Floch, P.-A. Duc, I. Mirabel, et al., *Astron. Astrophys.* 400, 499 (2003).
- S. Lilly, D. Schade, R. Ellis, et al., *Astrophys. J.* 500, 75 (1998).
- P. Madau, L. Pozzetti, and M. Dickinson, *Astrophys. J.* 498, 106(1998).
- T. Maihara, F. Iwamuro, H. Tanabe, et al., *Publ. Astron. Soc. J.* 53, 25 (2001).
- Sh. Mao, H. J. Mo, and S. D. M. White, *Mon. Not. R. Astron. Soc.* 297, L71 (1998).
- H. J. McCracken, M. Radovich, E. Bertin, et al., *Astron. Astrophys.* 410, 17 (2003).
- N. Metcalfe, T. Shanks, A. Campos, et al., *Mon. Not. R. Astron. Soc.* 323, 795 (2001).
- B. M. Poggianti, *Astron. Astrophys., Suppl. Ser.* 122, 399 (1997).
- E. Ramirez-Ruiz, E. Fenimore, and N. Trentham, *AIP Conf. Proc.* 555, 457 (2001).
- V. P. Reshetnikov, R.-J. Dettmar, and F. Combes, *Astron. Astrophys.* 399, 879 (2003).
- A. C. Robin, C. Reyle, and M. Creze, *Astron. Astrophys.* 359, 103 (2000).
- G. Rudnik, H.-W. Rix, M. Franx, et al., *astro-ph/0307149* (2003).
- M. Samland and O. E. Gerhard, *Astron. Astrophys.* 399, 961 (2003).
- L. Simard, D. C. Koo, S. M. Faber, et al., *Astrophys. J.* 519, 563 (1999).
- V. Sokolov, T. Fatkhullin, A. Castro-Tirado, et al., *Astron. Astrophys.* 372, 438 (2001).
- L. S. Sparke and J. S. Gallagher III, *Galaxies in the Universe: An Introduction* (Cambridge Univ. Press, Cambridge, 2000).
- A. Szalay, A. Connolly, and G. Szokoly, *Astron. J.* 177, 68 (1999).
- M. Takamiya, *Astrophys. J., Suppl. Ser.* 122, 109 (1999).
- N. Trentham, E. Ramirez-Ruiz, and A. Blain, *Mon. Not. R. Astron. Soc.* 334, 983 (2002).
- D. Schlegel, D. Finkbeiner, and M. Davis, *Astrophys. J.* 500, 525 (1998).
- P. Westera, M. Samland, R. Buser, and O. E. Gerhard, *Astron. Astrophys.* 389, 761 (2002).